



Possibilities of node location optimization and the quest isoparametric versus geometry-preserving approach in the collocation boundary element method

Ney A. Dumont¹

¹*Dept. of Civil and Environmental Engineering, Pontifical Catholic University of Rio de Janeiro
Rua Marquês de São Vicente 225, 22451900, Rio de Janeiro, Brazil*

Abstract. We have recently laid down the theoretical basis for the consistent formulation of the collocation boundary element method, as it should have been conceived from the beginning. We proved a convergence theorem for two- and three-dimensional problems of elasticity and potential, which applies to arbitrarily curved elements in the frame of an isoparametric analysis. We also showed that arbitrarily high precision and accuracy may be achieved. On the other hand, there still is the cost-benefit question of how to improve a real problem's simulation without refining too much a discretization mesh. The first possibility of doing this is optimizing the geometric location of the primary parameters (as for displacements and tractions, in elasticity) for the problem's mechanical description. This primarily consists in an hp-mesh refinement. We may also attach the problem's parameters to optimal locations inside the boundary element. A second issue is that an isoparametric formulation (generally in terms of polynomial interpolations along the boundary segment) may fail to reproduce the exact geometry of the idealized physical problem. Since, for two-dimensional problems, we have the boundary element formulation under control regarding all numerical evaluations, we assess how an isoparametric analysis compares to a formulation that preserves the problem's idealized geometry – in the context of a homothetic mesh generation. We present the conceptual formulation, and the basics for code implementation.

Keywords: Consistent boundary elements, Collocation, Isoparametric analysis, Geometry-preservation approach, Node location optimization, Homothetic mesh refinement

1 Introduction

Our recent proposition of the “consistent” collocation boundary element method (CBEM) has required a long maturation time since the first attempt of 30 years ago [1]. Some contributions followed sparsely [2–4] until the three-paper publication [5–7], which brought the theoretical basis for general linear problems of elastostatics and steady-state potential, with code-implementation and applications for the two-dimensional (2D) case. Although properly using the concept of “complex singularity poles”, these papers were based on real-variable Cartesian coordinates. A fully complex-variable reformulation followed quite recently [8], with friendlier equations and code implementation.

Despite the sound mathematics laid down in the papers just outlined, the question “can we do better?” (for the particular case of 2D linear problems of elastostatics and steady-state potential) persisted concerning the efficient numerical simulation in terms of eventually optimal node location inside a boundary element, efficient mesh-refinement, and accurate geometry representation.

This contribution is meant as the layout of a paper in preparation [9]. The denomination “geometry-preserving” is in the present context more informative than and not committed to the term “isogeometric” proposed by Hughes [10] for widespread applications also in the frame of the boundary element method – which do not take into account the mathematical consistency of our developments.

We first outline formulation and consistent notation for elastostatics [5–8, 11].

2 Basic problem formulation in the consistent CBEM

The basic system matrix to be solved in the frame of the CBEM has the format

$$\mathbf{H}(\mathbf{d} - \mathbf{d}^p) = \mathbf{G}(\mathbf{t} - \mathbf{t}^p)_{ad} \quad (1)$$

In this equation, \mathbf{H} is the square, double-layer potential matrix of order $n_d = 2n_n$, for 2D elasticity and the problem discretized with n_n nodal points, and \mathbf{G} is the single-layer potential matrix with $2n_n$ rows and $2(n_n + n_e)$ columns, as we code for n_e elements of any order o_e , in principle taking into account that the left and right tangents at a nodal point connecting two elements are different, in the isoparametric formulation for generally curved boundaries. The number of columns of \mathbf{G} may be significantly smaller in the patch-related, geometry-preserving formulation we are about to present.

As laid down in [5], we are assuming just for the sake of elegant and compact formulation that some *particular* solution of interest is known – whether or not related to non-zero body forces – and may be approximately expressed as boundary nodal displacement \mathbf{d}^p and traction \mathbf{t}^p data [11, 12]. The problem’s primary boundary displacement and traction parameters are \mathbf{d} and \mathbf{t} , which are in part known and in part to be obtained in the frame of a general mixed-boundary formulation. As comprehensively assessed in [3, 5–7], we write for consistency that the traction $(\mathbf{t} - \mathbf{t}^p)_{ad}$ is *admissible*, in equilibrium with the applied domain forces: this follows the same mathematical/mechanical principle that, since – for a finite domain – rigid-body displacement amounts of $(\mathbf{d} - \mathbf{d}^p)$ cannot be transformed into forces, also non-equilibrated forces should not be transformed into displacements (see Section 4.3).

In two-dimensional, complex-variable plane-strain elasticity, the matrices of eq. (1) are [8]

$$G_{s\ell} = \int_{\Gamma} \begin{bmatrix} -(3-4\nu) \ln(z\bar{z}) & \frac{z}{\bar{z}} \\ \frac{\bar{z}}{z} & -(3-4\nu) \ln(z\bar{z}) \end{bmatrix} \frac{|J|_{(at\ell)} N_{\ell}^{o_e} d\xi}{16\pi G (1-\nu)} \quad (2)$$

$$H_{sn} = \int_{\Gamma} \begin{bmatrix} (3-4\nu) \frac{z'}{z} - \frac{\bar{z}'}{\bar{z}} & \frac{z'}{\bar{z}} - \frac{z}{\bar{z}^2} \bar{z}' \\ -\frac{\bar{z}'}{z} + \frac{\bar{z}}{z^2} z' & \frac{z'}{z} - (3-4\nu) \frac{\bar{z}'}{\bar{z}} \end{bmatrix} \frac{i N_n^{o_e} d\xi}{8\pi (1-\nu)} + \delta_{sn} \quad (3)$$

Real-variable expressions [6] might substitute for the above, but the complex representation is much simpler. Here, $z = x + iy$, and we use $n = -iz'/|J| \Leftrightarrow \bar{n} = iz'/|J|$ for the unit normal, also considering $d\Gamma = |J|d\xi$. The material’s shear modulus and Poisson’s ratio are G and ν .

The rows above refer to the *source*, complex point force $p_s^* = (p_x^* + i p_y^*)|_{(at\ s)}$ and its conjugate $\bar{p}_s^* = (p_x^* - i p_y^*)|_{(at\ s)}$. The first columns stand for either *node* n or *locus* ℓ on a boundary segment, to which either complex displacements $d_n = (d_x + i d_y)|_{(at\ n)}$ or tractions $t_{\ell} = (t_x + i t_y)|_{(at\ \ell)}$ are attached. Only the first rows of the above matrices need to be implemented in a code [8].

We develop eqs. (2) and (3) for evaluations using Gauss-Legendre quadrature and then eventually accrue mathematically exact corrections conditioned by three logical constants $\langle no_sing, sing, quasi_sing \rangle$. This is thoroughly addressed in [8, 11].

3 Consistent notation and implementation possibilities

Displacement and traction representation. The real functions $N_n^{o_e} \equiv N_n^{o_e}(\xi)$ and $N_\ell^{o_e} \equiv N_\ell^{o_e}(\xi)$ of the real, natural variable $\xi \in [0, 1]$ interpolate displacements and tractions, respectively, along a generic boundary segment $\Gamma_{seg} \equiv \Gamma_{seg}(\xi)$, $\xi \in [0, 1]$, of the problem's whole boundary Γ . This is carried out in the frame of a *consistent* formulation of the CBEM [5–8, 11]. The functions $N_n^{o_e}$ interpolate displacements from *nodal* displacements d_n , whereas $N_\ell^{o_e}$ interpolate from traction parameters attached to boundary *loci*. Such *nodes* n and *loci* ℓ are different geometric entities that may be differently allocated along the boundary. The superscript o_e in both $N_n^{o_e}$ and $N_\ell^{o_e}$ is the interpolation order of the Lagrangian polynomials, as previously considered. Our codes are implemented for the four cases $o_e = 1, 2, 3, 4$.

Isoparametric boundary geometry description. We also recognize in eqs. (2) and (3) the boundary geometry description given by the complex $z \equiv z(\xi) - z_s = x(\xi) - x_s + i(y(\xi) - y_s)$, then referred to a *source* point s that may be infinitesimally close to but is conceptually not on the boundary [5]. In an isoparametric formulation, the boundary Cartesian coordinates (x, y) are interpolated along each boundary segment Γ_{seg} in terms of interpolation functions $N_m^{o_e}$ (m refers to key geometric points) that are linear combinations of the displacement interpolation functions $N_n^{o_e}$.

Schematic illustration. We illustrate on the left in Figure 1 – as already advanced in [11] – the case of two consecutive cubic ($o_e = 3$) boundary elements of a 2D elasticity problem, with $n_m = n_n = 4$ *nodes* for geometry (\circ) and displacements (\odot), which in this case coincide (as it usually occurs in an isoparametric formulation), and $n_\ell = n_n = 4$ *loci* (\times) for tractions, which are not at the element extremities but at distances $\epsilon \rightarrow 0$ (we do not say “discontinuous”, which is just a misconception [5]). The *points* ($*$) are for the collocation of the sources s in the domain but at distances $\rightarrow 0$ from the nodal points n , in the frame of the CBEM. There are $n^d = n^{el}(n_n - 1) = 3n^{el}$ nodes for a total of n^{el} elements that comprise the complete problem we are simulating with cubic elements. For an elasticity problem implemented in terms of real variables, the double-layer potential matrix \mathbf{H} is square of order $2n^d = 2n^{el}(n_n - 1) = 6n^{el}$, and the single-layer potential matrix \mathbf{G} has the same number of rows but $2n^t = 2n^{el}n_\ell = 8n^{el}$ columns, where n^t is the total number of traction *loci*.

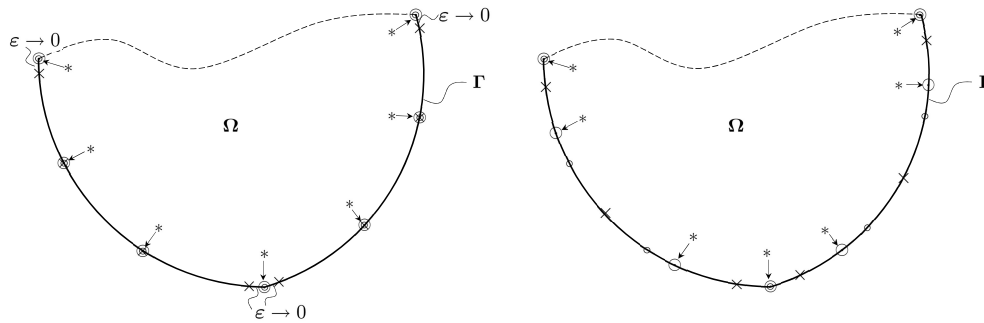


Figure 1. Two consecutive cubic elements, on the left for $n_m = n_n = n_\ell = 4$ *nodes* and *loci* per element, and on the right in an optimization attempt for $n_m = n_n = 4$ *nodes* and $n_\ell = 3$ *loci* [9, 11].

3.1 Attempt to optimize *node* n and *locus* ℓ locations inside an isoparametric element

The case on the right in Fig. 1 is almost similar to the previous description, also with $n_m = n_n = 4$ *nodes* for geometry and displacements, but whose locations only coincide at the extremities, since we are now considering the abscissas of a Radau-Lobatto quadrature for the displacement nodes (\odot) while

keeping the geometry nodes (\circ) unaltered. Most important, we have $n_\ell = n_n - 1 = 3$ parameter *loci* (\times) for traction along an element at abscissas given by the roots of a Legendre polynomial, which are at finite distances from the element extremities: such implementation still satisfies the convergence Theorem 1 [5]. There are in this case $n^d = n^t = n^{el}(n_n - 1) = 3n^{el}$ nodes and *loci* for a total of n^{el} elements. In terms of real variables, both matrices \mathbf{G} and \mathbf{H} are square of order $2n^d = 2n^{el}(n_n - 1) = 6n^{el}$.

The reason for such an implementation would be to improve the representation capacity of interpolation functions N_n^{oe} and N_ℓ^{oe} , as n_n Radau-Lobatto and n_ℓ Legendre points lead to the accurate integral representation of polynomials of order $2n_n - 3$ and $2n_\ell - 1$, respectively. In the illustrative case of a cubic (order 3) element, we have $2 \times 4 - 3 = 5$ and $2 \times 3 - 1 = 5$, thus 5th (and not just 3rd) order polynomial representations for displacements and tractions.

Such an idea of polynomial optimization seems tempting and may deserve some numerical experiments (we already have the code implementation). However, there are some issues to consider. First, the polynomials N_ℓ^{oe} and N_n^{oe} do not feature alone in a boundary element implementation, but rather multiplied with some functions, as given in eqs. (2) and (3). Then, the integral representation capacity referred to in the above paragraph – and the basis of the Gauss-Legendre quadrature – does not take place in the applications of interest. A second, not strong reasoning would be in terms of result interpretation, as the n_n and n_ℓ locations are not as simply distributed as in the scheme on the left in Fig. 1. There is, however, a very strong argument against such an optimization attempt, which is related to the lack of smoothness in the distribution of n_n and n_ℓ locations along a boundary patch – particularly in the frame of an adaptive mesh refinement, as we address next.

4 The concept of geometry-preserving boundary patches Γ_{patch}

4.1 Homothetic node and element generation

Figure 2 represents a general patch that spans from (x_{init}, y_{init}) to (x_{final}, y_{final}) and has the shape $(x_{patch}(\zeta) = \Delta\zeta, y_{patch}(\zeta))$, $\zeta \in [0, 1]$ where $y_{patch}(\zeta)$ must be entered.

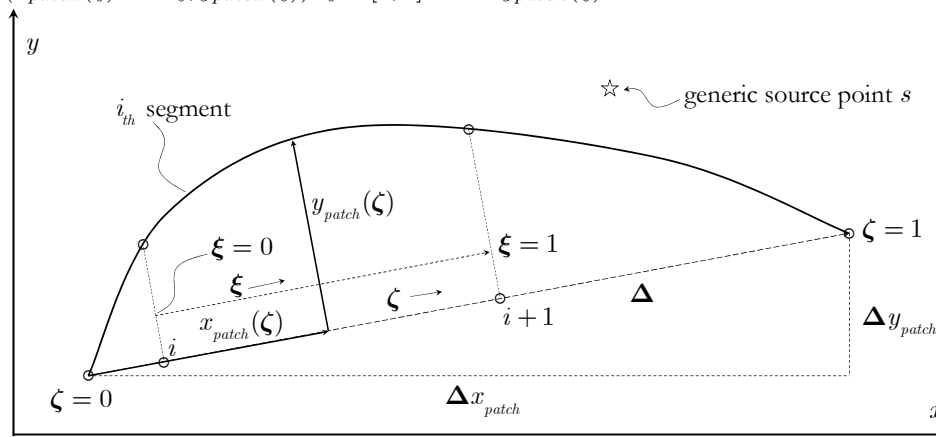


Figure 2. Generic boundary patch $\Gamma_{patch}(\zeta)$, $\zeta \in [0, 1]$ with a segment $\Gamma_{seg}(\xi)$, $\xi \in [0, 1]$ [9, 11].

We may have any topologically consistent boundary shape $y_{patch}(\zeta)$, $\zeta \in [0, 1]$, in which “consistent” means that the Jacobian of the coordinate transformation keeps positive not only along the curved boundary but also in the complex vicinity, for the analytical corrections of eventual quasi singularities [5–8, 11] to take place. The global coordinates are, in terms of the complex $z(\zeta) = x(\zeta) + iy(\zeta)$,

$$z(\zeta) = z_{init} + z_{patch}(\zeta)\Delta z_{patch}/\Delta \quad (4)$$

In the code implementation, the outer-most loop runs for the boundary patches, $i_{patch} = 1 \dots n_{patch}$, with geometry pre-evaluations carried out and stored for a typical element of the patch, as shown next [9], which includes adaptive mesh refinement along a patch within the concept of *homothetic elements*. Only then we run a loop for the source points s , evaluate the patch-related complex distance ζ_s , and then have the loop for all elements inside the patch, again, for which the pre-evaluations have been done.

Figure 3 is the schematic illustration of how homothetic elements are generated, with meshes going from node 1 through node 13, for the generation of 6 quadratic or 3 quartic elements including internal natural points $\xi_j, j = 2 \dots o_e$, as we always have $\xi_1 = 0$ and $\xi_{o_e+1} = 1$. Nodes 2 through 12 are generated in such a way that the distance between consecutive nodes increases at a geometric rate $f_{node} = 1.25$. The relative size f_{el} of consecutive elements also increases exponentially:

$$f_{el} = f_{node}^{o_e} \quad (5)$$

This means that the node locations inside any element of the patch have the same representation in terms of the element natural coordinate $\xi \in [0, 1]$, which is illustratively shown for some elements in the figure. This is the reason of calling “homothetic” such combined element and node generation. Given a boundary patch i_{patch} , we first carry out all necessary geometric and singularity-related pre-evaluations for a representative element of the patch and only then proceed with the algorithm that takes the source points into account. These pre-evaluations include the analytical expression and storage of $N_n^{o_e}$ and $N_\ell^{o_e}$ as well as of the integrals required in the quasi-singularity corrections – always taking into account that the natural node coordinates $\xi_j, j = 1 \dots o_e+1$ are not equally spaced inside the element but rather reflect the distance amplification illustrated in Fig. 3. This means, for instance, that the Jacobian for coordinate transformations along straight and circular patches is constant, which leads to smaller quadrature errors.

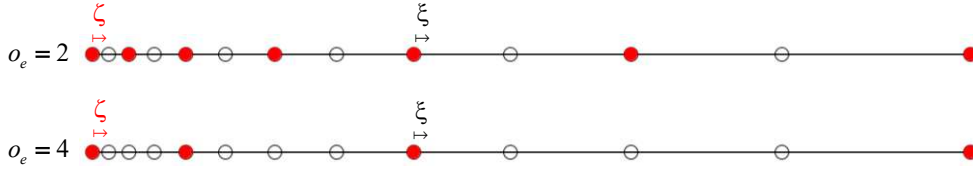


Figure 3. Schematics of a boundary patch (coordinates $\zeta \in [0, 1]$) with 13 nodes (circles), whose consecutive distances grow at the rate $f_{node} = 1.25$. Homothetic subdivision for quadratic and quartic elements (coordinates $\xi_j \in [0, 1]$, solid circles for the respective extremity nodes) is also indicated [9, 11].

Let n_ζ be the numbering difference between the first and last nodes of a patch. We set

$$\tilde{\zeta} = 1 \left/ \sum_{j=0}^{n_\zeta-1} f_{node}^j \right., \quad \delta = 0 \quad (6)$$

and carry out the algorithm for the evaluation of the local ζ_i coordinates of the generated nodes:

$$\text{for } i \text{ from } 1 \text{ to } n_\zeta + 1 \text{ do } \quad \zeta_i = \delta \tilde{\zeta}; \quad \delta \leftarrow \delta f_{node} + 1; \quad \text{end do} \quad (7)$$

The coordinate transformation between patch coordinate ζ and element coordinate ξ is given for the i -th element, according to Fig. 3, as

$$\zeta = \zeta_i + \xi (\zeta_{i+1} - \zeta_i) \quad \Leftrightarrow \quad \xi = (\zeta - \zeta_i) / (\zeta_{i+1} - \zeta_i), \quad \zeta \in [\zeta_i, \zeta_{i+1}] \quad (8)$$

and the Jacobian $|J(\zeta)| \equiv |\partial z(\zeta) / \partial \zeta|$ of the coordinate transformation is

$$|J(\xi)|_{seg} = |J(\zeta)|_{patch} \left. \frac{\partial \zeta}{\partial \xi} \right|_{seg} = |J(\zeta)|_{patch} (\zeta_{i+1} - \zeta_i), \quad \zeta \in [\zeta_i, \zeta_{i+1}] \quad (9)$$

4.2 Evaluation of the complex ζ_s coordinate of a quasi-singular point source $z_s = x_s + iy_s$

Figure 2 depicts a *star* for a generic source point, which may be extremely close to the boundary [5–8, 11, 12]. In these papers, the complex natural coordinate ξ_s corresponding to a close source point $z_s = x_s + iy_s$ is evaluated iteratively for every boundary segment Γ_{seg} , as its geometry is given – in the frame of an isoparametric formulation – piecewise in terms of the interpolation functions $N_n^{oe}(\xi)$ with local support $\xi \in [0, 1]$. In the present geometry-preserving formulation, we have a unique analytical function $z(\zeta)$ spanning a whole boundary patch, according to eq. (4). The search is then for the patch-related complex natural coordinate ζ_s in terms of the same Newton-Raphson algorithm outlined in Appendix A of [5]. Once obtained for a given patch $\Gamma_{patch}(\zeta)$, ζ_s is successively transformed into the complex ξ_s for each one of the boundary segments $\Gamma_{seg}(\xi)$ according to the same eq. (8), where both ζ_s and ξ_s are in general complex. When the boundary patch is either a straight segment or an arc of circle, the natural coordinates ζ and ξ of the general Fig. 2 are defined as following along the curved patch, leading to a constant Jacobian even for adaptive mesh refinement. In such particular cases, the complex source point ζ_s may be obtained analytically, which speeds up calculations [9].

4.3 Spaces \mathbf{W} , \mathbf{R} of inadmissible displacements and tractions

Rigid-body displacements. We have proposed at the very beginning of our developments on boundary element methods [13] a matrix \mathbf{W} as the basis of rigid-body displacements in a finite domain, as expressed for elasticity. This is shown in detail in [5], where it is set in eq. (18) of **Definition 1** that the rigid-body displacements u_{ik}^r along the boundary are linear combinations of the displacements N_n^{oe} – see [8] for the complex representation of \mathbf{W} . However, this only holds in the isoparametric formulation.

Inadmissible tractions. A *consistent* boundary element formulation requires that, for a finite body, if the rigid-body amount of displacements ($\mathbf{d} - \mathbf{d}^p$) in eq. (1) cannot be transformed into forces, conversely, the amount of non-equilibrated tractions ($\mathbf{t} - \mathbf{t}^p$) cannot be transformed into displacements [3, 5, 8, 11]:

$$\mathbf{H}\mathbf{W} = \mathbf{0} \quad \Leftrightarrow \quad \mathbf{G}_{ad}\mathbf{R} = \mathbf{0} \quad (10)$$

This leads to the evaluation of the rigid-body displacement amount in the expression of a fundamental solution, embedded in the single-layer potential matrix \mathbf{G}_{ad} , where the subscript means the filtered, *admissible* part of the matrix [3, 5]. The formulation in terms of a complex variable is shown in Appendix A.2.2 of [8]. In the case of a geometry-preserving formulation, we carry the following Gauss-Legendre quadrature along each segment of the whole boundary, where \mathbf{W} is the indicated array [9]:

$$R_{\ell k} = |J|_{(\text{at } \ell)} \int_0^1 \begin{bmatrix} 1 & i & iz(\zeta(\xi)) \\ 1 & -i & -i\bar{z}(\zeta(\xi)) \end{bmatrix} N_{\ell}^{oe}(\xi) d\xi \quad \text{for a boundary element} \quad (11)$$

5 Conclusions

The developments proposed in [8, 12] as the complex-variable counterpart of [5–7] for 2D potential and elasticity problems could be further improved, as shown in this short contribution – on conceptual ideas only – and to be numerically assessed in a paper in preparation [9]. Further to properly addressing the three entities – *boundary nodes* n (for potentials or displacements), *boundary loci* ℓ (to which normal fluxes or tractions are referred), and *domain points* s , at which we collocate the singular sources in the context of an isoparametric formulation – we show that a *geometry-preserving* concept must be explicitly

resorted to if numerical precision and accuracy are deemed relevant in the numerical simulation of real-world problems – particularly when dealing with topologically challenging configurations. We introduce the concept of *geometry-preserving boundary patches* Γ_{patch} , along which boundary nodes and elements are adaptively refined in a *homothetic* approach [9].

Acknowledgements. This project was supported by the Brazilian federal agencies CAPES and CNPq, as well as by the state agency FAPERJ.

Authorship statement. The author hereby confirms that he is the sole liable person responsible for the authorship of this work, and that all material that has been herein included as part of the present paper is the property (and authorship) of the author.

References

- [1] N. A. Dumont. On the efficient numerical evaluation of integrals with complex singularity poles. *Engineering Analysis with Boundary Elements*, vol. 13, pp. 155–168, 1994.
- [2] N. A. Dumont and M. Noronha. A simple, accurate scheme for the numerical evaluation of integrals with complex singularity poles. *Computational Mechanics*, vol. 22, n. 1, pp. 42–49, 1998.
- [3] N. A. Dumont. An assessment of the spectral properties of the matrix G used in the boundary element methods. *Computational Mechanics*, vol. 22, n. 1, pp. 32–41, 1998.
- [4] N. A. Dumont. The collocation boundary element method revisited: Perfect code for 2D problems. *International Journal of Computational Methods and Experimental Measurements*, vol. 6, n. 6, pp. 965–975, 2018.
- [5] N. A. Dumont. The consistent boundary element method for potential and elasticity: Part I — formulation and convergence theorem. *EABE - Engineering Analysis with Boundary Element Methods*, vol. 149, pp. 127–142, 2023a.
- [6] N. A. Dumont. The consistent boundary element method for potential and elasticity: Part II — machine-precision numerical evaluations for 2D problems. *EABE - Engineering Analysis with Boundary Element Methods*, vol. 149, pp. 92–111, 2023b.
- [7] N. A. Dumont. The consistent boundary element method for potential and elasticity: Part III — topologically challenging numerical assessments for 2D problems. *Engineering Analysis with Boundary Element Methods*, vol. 151, pp. 548–564, 2023c.
- [8] N. A. Dumont. Complex-variable, high-precision formulation of the consistent boundary element method for 2D potential and elasticity problems. *Engineering Analysis with Boundary Element Methods*, vol. 152, pp. 552–574, 2023d.
- [9] N. A. Dumont. Consistent boundary element method for two-dimensional problems with geometry-preserving, homothetic element generation. *EABE - Engineering Analysis with Boundary Element Methods*. To be submitted, 2024a.
- [10] J. A. Cottrell, T. J. R. Hughes, and Y. Bazilevs. *Isogeometric Analysis: Toward Integration of CAD and FEA*. John Wiley and Sons, 2009.
- [11] N. A. Dumont. Consistency, precision, and accuracy assessment of the collocation boundary element method for two-dimensional problems of potential and elasticity. *Archive of Applied Mechanics*, 2024b.
- [12] N. A. Dumont. Real- and complex-variable implementations of the consistent boundary element method in two-dimensional elasticity: a comparative assessment. In *Boundary Elements and Other Mesh Reduction Methods XLVI*, pp. 55–66. WITPress. Eds: A. H. D. Cheng and E. Divo and A. Kassab and S. Syngellakis, 2023e.
- [13] N. A. Dumont. The hybrid boundary element method: an alliance between mechanical consistency and simplicity. *Applied Mechanics Reviews*, vol. 42, n. 11, pp. S54–S63, 1989.